Computers and Structures 139 (2014) 54–64

Contents lists available at ScienceDirect

Computers and Structures

journal homepage: www.elsevier.com/locate/compstruc

Estimating relative eigenvalue errors in the Craig-Bampton method

Jin-Gyun Kim, Kang-Heon Lee, Phill-Seung Lee *

Division of Ocean Systems Engineering, Korea Advanced Institute of Science and Technology, 291 Daehak-ro, Yuseong-gu, Daejeon 305-701, Republic of Korea

ARTICLE INFO

Article history:
Received 18 December 2013
Accepted 18 April 2014

Keywords:
Structural dynamics
Finite element method
Model reduction
Component mode synthesis
Error estimation
Eigenvalue problem

ABSTRACT

In this study, we propose an accurate error estimator for the Craig-Bampton (CB) method, which is a widely used component mode synthesis (CMS) method. The proposed error estimator can precisely predict relative eigenvalue errors in finite element models reduced by the CB method. To develop the error estimator, we propose an enhanced transformation matrix for the CB method and, using the transformation matrix, the error estimator is derived from the global (original) eigenvalue problem. In this paper, we demonstrate the robustness of the proposed error estimator through various numerical examples.

1. Introduction

In structural engineering, the numerical analysis of large finite element models requires considerably high computational cost. This has motivated the development of the reduced-order modeling techniques. Component mode synthesis (CMS) is a widely used reduced-order modeling technique in structural dynamics. In CMS methods, a large structural model is partitioned into small substructures and then is approximated by a reduced model constructed by using only dominant substructural modes. Since we deal with the reduced and small substructural models instead of the large model, CMS methods can dramatically reduce computational cost. In the 1960s, Craig and Bampton [1] proposed the initial concept of CMS methods based on Hurty and Guyan's ideas [2,3], and, since then, various methods have been developed (see, e.g., Refs. [4–13]).

An important issue in CMS methods is how to evaluate the reliability of the reduced model compared to the global (original) model. Although the reliability of the reduced model can be directly assessed by errors in its approximated global eigenvalues, it is basically difficult to calculate the errors because the exact global eigenvalues are unknown. To handle this issue, various error estimation methods have been developed (see, e.g., Bourquin [14], Yang et al. [15], Elssel and Voss [16], Jakobsson and Larson [17], Kim and Lee [18]). However, those error estimation methods show qualitative tendencies rather than meaningful quantities in eigenvalue errors.

In order to accurately estimate individual eigenvalue errors in reduced models, we here propose an error estimator. The error estimator is derived from the global (original) eigenvalue problem, in which the global eigenvalue and eigenvector are divided into approximated and error parts and a newly defined transformation matrix $\bar{\mathbf{T}}_1$ is used to approximate the global eigenvector in the CB method.

In the original CB formulation, the transformation matrix $\bar{\mathbf{T}}_0$ is constructed by using only dominant substructural modes, and the residual substructural modes are truncated without any consideration. However, considering the residual substructural modes, the transformation matrix $\bar{\mathbf{T}}_0$ can be enhanced. Therefore, when the enhanced transformation matrix $\bar{\mathbf{T}}_1$ is used instead of the original one, the global eigenvectors can be approximated more accurately.

The derivation procedure shows that the relative eigenvalue error can be approximated by the proposed error estimator. To evaluate the error estimator proposed, no heavy computation is required. That is, only simple additions and multiplications of known matrices are necessary.

In Section 2, the general description of CMS methods and the original CB method are briefly reviewed and the formulation details of the enhanced transformation matrix are presented in Section 3. In Section 4, we derive the error estimator. Its performance is tested through various numerical examples in Section 5. The conclusions are given in Section 6.

* Corresponding author. Tel.: +82 42 350 1512; fax: +82 42 350 1510.
E-mail addresses: jingyun@kaist.ac.kr (J.-G. Kim), welcome@kaist.ac.kr (K.-H. Lee), phillseung@kaist.edu (P.S. Lee).

http://dx.doi.org/10.1016/j.compstruc.2014.04.008
0045-7949/

2. Craig-Bampton method

In this section, we briefly introduce the general description of component mode synthesis (CMS), and review the formulation of the Craig-Bampton (CB) method.

2.1. General description of the CMS methods

Considering the global (non-partitioned) structure Ω modeled by finite element discretization in Fig. 1(a), the linear dynamics equations without damping can be expressed by

$$\mathbf{M}_g\ddot{\mathbf{u}}_g + \mathbf{K}_g\mathbf{u}_g = \mathbf{f}_g, \tag{1}$$

where $\mathbf{M}_g$ and $\mathbf{K}_g$ are the global mass and stiffness matrices, respectively, $\mathbf{u}_g$ is the global displacement vector, and $\mathbf{f}_g$ is the global force vector. The subscript g denotes the global structure, and $(\ddot{}) = d^2(\ )/dt^2$.

The generalized eigenvalue problem of the global structure is

$$\mathbf{K}_g(\boldsymbol{\phi}_g)_i = \lambda_i\mathbf{M}_g(\boldsymbol{\phi}_g)_i, \quad i = 1,2,\ldots,N_g, \quad \text{with } \mathbf{u}_g = \boldsymbol{\Phi}_g\mathbf{q}_g, \tag{2}$$

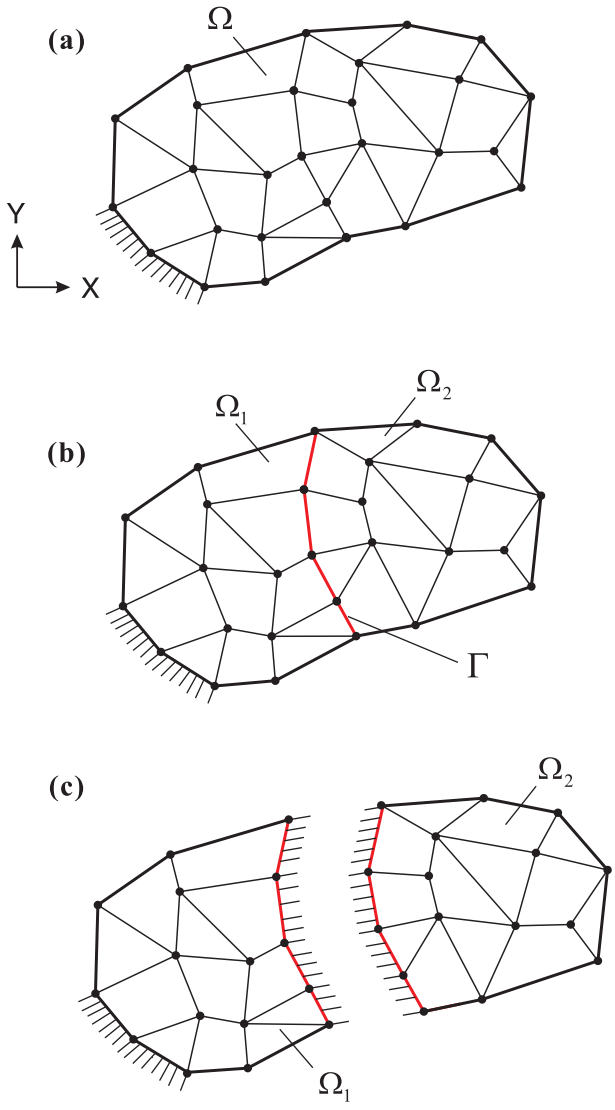

Fig. 1. Global and partitioned structural models and interface handling in the CB method. (a) Global (non-partitioned) structure Ω, (b) Partitioned structure, $\Omega = \Omega_1 \cup \Omega_2$, $\Gamma = \Omega_1 \cap \Omega_2$, (c) Interface boundary treatment.

where λ_i and $(\boldsymbol{\phi}_g)_i$ are the eigenvalue and eigenvector calculated in the global structure, respectively, N_g is the number of DOFs in the global structure, and $\boldsymbol{\Phi}_g$ and $\mathbf{q}_g$ are the global eigenvector matrix and its generalized coordinate vector, respectively. Note that λ_i and $(\boldsymbol{\phi}_g)_i$ are the square of the ith natural frequency (ω^2) and the corresponding mode in structural dynamics, respectively.

The eigensolutions λ_i and $(\boldsymbol{\phi}_g)_i$ satisfy the following relations:

$$(\boldsymbol{\phi}_g)_i^T\mathbf{M}_g(\boldsymbol{\phi}_g)_j = \delta_{ij} \quad \text{for } i \text{ and } j = 1,2,\ldots,N_g, \tag{3a}$$

$$(\boldsymbol{\phi}_g)_i^T\mathbf{K}_g(\boldsymbol{\phi}_g)_j = \lambda_j\delta_{ij} \quad \text{for } i \text{ and } j = 1,2,\ldots,N_g, \tag{3b}$$

where δ_{ij} is the Kronecker delta ($\delta_{ij} = 1$ if $i = j$, otherwise $\delta_{ij} = 0$). The conditions in Eqs. (3a) and (3b) are called "mass-orthonormality" and "stiffness-orthogonality", respectively.

In the CMS methods, the global structure is partitioned into substructures as shown Fig. 1(b), and the eigenvalue analyses of individual substructures are carried out. Among the calculated substructural modes, dominant substructural modes are selected and the reduced eigenvalue problem is constructed using the selected substructural modes

$$\bar{\mathbf{K}}_p(\bar{\boldsymbol{\phi}}_p)_i = \bar{\lambda}_i\bar{\mathbf{M}}_p(\bar{\boldsymbol{\phi}}_p)_i, \quad i = 1,2,\ldots,\overline{N}_p, \quad \text{with } \bar{\mathbf{u}}_p = \bar{\boldsymbol{\Phi}}_p\bar{\mathbf{q}}_p, \tag{4}$$

where $\bar{\mathbf{M}}_p$ and $\bar{\mathbf{K}}_p$ are the reduced mass and stiffness matrices, respectively, and $\bar{\lambda}_i$ and $(\bar{\boldsymbol{\phi}}_p)_i$ are the approximated eigenvalue and eigenvector, respectively. $\overline{N}_p$ is the number of DOFs in the reduced model and $\bar{\mathbf{u}}_p$ is the approximated displacement vector defined by the approximated eigenvector matrix $\bar{\boldsymbol{\Phi}}_p$ and the generalized coordinate vector $\bar{\mathbf{q}}_p$. Note that the subscript p denotes the partitioned structure and an overbar $\bar{}$ denotes the approximated quantities.

The approximated eigensolutions $\bar{\lambda}_i$ and $(\bar{\boldsymbol{\phi}}_p)_i$ satisfy the following relations:

$$(\bar{\boldsymbol{\phi}}_p)_i^T\bar{\mathbf{M}}_p(\bar{\boldsymbol{\phi}}_p)_j = \delta_{ij} \quad \text{for } i \text{ and } j = 1,2,\ldots,\overline{N}_p, \tag{5a}$$

$$(\bar{\boldsymbol{\phi}}_p)_i^T\bar{\mathbf{K}}_p(\bar{\boldsymbol{\phi}}_p)_j = \bar{\lambda}_j\delta_{ij} \quad \text{for } i \text{ and } j = 1,2,\ldots,\overline{N}_p. \tag{5b}$$

Since the approximated global eigenvector matrix $\bar{\boldsymbol{\Phi}}_g$ and its generalized coordinate vector $\bar{\mathbf{q}}_g$ can be calculated from $\bar{\boldsymbol{\Phi}}_p$ and $\bar{\mathbf{q}}_p$ in Eq. (4), we finally obtain the reduced form of Eq. (1) in the generalized coordinates

$$\begin{aligned}
&\ddot{\bar{\mathbf{q}}}_g + \bar{\boldsymbol{\Lambda}}_p\bar{\mathbf{q}}_g \approx \bar{\mathbf{f}}_g,\\
&\bar{\boldsymbol{\Phi}}_g^T\mathbf{M}_g\bar{\boldsymbol{\Phi}}_g \approx \mathbf{I}_p, \quad \bar{\boldsymbol{\Phi}}_g^T\mathbf{K}_g\bar{\boldsymbol{\Phi}}_g \approx \bar{\boldsymbol{\Lambda}}_p,\\
&\bar{\boldsymbol{\Lambda}}_p = \mathrm{diag}(\bar{\lambda}_1,\bar{\lambda}_2,\ldots\bar{\lambda}_i\ldots,\bar{\lambda}_{\bar{N}_p}), \quad \bar{\mathbf{f}}_g = \bar{\boldsymbol{\Phi}}_g^T\mathbf{f}_g,
\end{aligned} \tag{6}$$

where $\mathbf{I}_p$ is the $\bar{N}_p \times \bar{N}_p$ identity matrix. While the formulation details may differ considerably among various CMS methods, the general descriptions are similar.

2.2. Original formulation of the CB method

The CB method is a popular and widely used CMS method [1]. In the CB method, substructures are connected with a fixed interface at the interface boundary Γ, see Fig. 1(b). After partitioning the global structure into N_s substructures,

Eq. (1) can be represented by separating into substructural (or interior) and interface boundary parts

$$\mathbf{M}_g = \begin{bmatrix}\mathbf{M}_s & \mathbf{M}_c\\ \mathbf{M}_c^T & \mathbf{M}_b\end{bmatrix}, \quad \mathbf{K}_g = \begin{bmatrix}\mathbf{K}_s & \mathbf{K}_c\\ \mathbf{K}_c^T & \mathbf{K}_b\end{bmatrix}, \quad \mathbf{u}_g = \begin{bmatrix}\mathbf{u}_s\\ \mathbf{u}_b\end{bmatrix}, \quad \mathbf{f}_g = \begin{bmatrix}\mathbf{f}_s\\ \mathbf{f}_b\end{bmatrix}, \tag{7}$$

in which the subscripts s and b denote the substructural and interface boundary quantities, respectively, and c denotes the coupling quantities. $\mathbf{M}_s$ and $\mathbf{K}_s$ are the partitioned block diagonal mass and stiffness matrices that consist of substructural mass and stiffness matrices ($\mathbf{M}_s^{(k)}$ and $\mathbf{K}_s^{(k)}$).

In the CB method, the global displacement vector $\mathbf{u}_g$ can be defined by

$$\mathbf{u}_g = \begin{bmatrix} \mathbf{u}_s \\ \mathbf{u}_b \end{bmatrix} = \mathbf{T}_0 \begin{bmatrix} \mathbf{q}_s \\ \mathbf{u}_b \end{bmatrix}, \quad \mathbf{T}_0 = \begin{bmatrix} \mathbf{\Phi}_s & -\mathbf{K}_s^{-1}\mathbf{K}_c \\ \mathbf{0} & \mathbf{I}_b \end{bmatrix}, \tag{8}$$

where $\mathbf{q}_s$ is the generalized coordinate vector for the substructural modes, $\mathbf{T}_0$ is the transformation matrix, and $\mathbf{I}_b$ is an identity matrix for the interface boundary. $\mathbf{\Phi}_s$ is a block diagonal eigenvector matrix calculated from the following substructural eigenvalue problems

$$[\mathbf{K}_s^{(k)} - \lambda_i^{(k)}\mathbf{M}_s^{(k)}](\boldsymbol{\phi}^{(k)})_i = \mathbf{0}, \quad i = 1,2,\ldots,N_q^{(k)}, \quad \text{for } k = 1,2,\ldots,N_s, \tag{9}$$

where $N_q^{(k)}$ is the number of deformable modes in the kth substructure, and $\lambda_i^{(k)}$ and $(\boldsymbol{\phi}^{(k)})_i$ are the substructural eigensolutions.

The substructural displacement vector $\mathbf{u}_s$ can be decomposed into the dominant and residual modes

$$\mathbf{u}_s = \mathbf{\Phi}_s\mathbf{q}_s - \mathbf{K}_s^{-1}\mathbf{K}_c\mathbf{u}_b = [\mathbf{\Phi}_d \quad \mathbf{\Phi}_r]\begin{bmatrix} \mathbf{q}_d \\ \mathbf{q}_r \end{bmatrix} - \mathbf{K}_s^{-1}\mathbf{K}_c\mathbf{u}_b, \tag{10}$$

where $\mathbf{\Phi}_d$ and $\mathbf{\Phi}_r$ are the dominant and residual substructural eigenvector matrices, respectively, and $\mathbf{q}_d$ and $\mathbf{q}_r$ are the corresponding generalized coordinate vectors. The subscripts d and r denote the dominant and residual terms, respectively. In general, a small number of the dominant modes is used to reduce the global structure. That is, $N_d \ll N_r$, in which N_d and N_r are the numbers of the dominant and residual modes, respectively.

Neglecting the residual modes in Eq. (10), the global displacement vector $\mathbf{u}_g$ is approximated by

$$\mathbf{u}_g \approx \bar{\mathbf{u}}_g = \bar{\mathbf{T}}_0 \begin{bmatrix} \mathbf{q}_d \\ \mathbf{u}_b \end{bmatrix}, \quad \bar{\mathbf{T}}_0 = \begin{bmatrix} \mathbf{\Phi}_d & -\mathbf{K}_s^{-1}\mathbf{K}_c \\ \mathbf{0} & \mathbf{I}_b \end{bmatrix}, \tag{11}$$

where $\bar{\mathbf{T}}_0$ is the reduced transformation matrix. Using Eq. (11) in Eq. (7), we can obtain the reduced equations of motion for the partitioned structure

$$\begin{aligned} &\bar{\mathbf{M}}_p\ddot{\bar{\mathbf{u}}}_p + \bar{\mathbf{K}}_p\bar{\mathbf{u}}_p = \bar{\mathbf{f}}_p, \\ &\bar{\mathbf{M}}_p = \bar{\mathbf{T}}_0^T\mathbf{M}_g\bar{\mathbf{T}}_0 = \begin{bmatrix} \mathbf{I}_d & \bar{\mathbf{M}}_c \\ \bar{\mathbf{M}}_c^T & \hat{\mathbf{M}}_b \end{bmatrix}, \quad \bar{\mathbf{K}}_p = \bar{\mathbf{T}}_0^T\mathbf{K}_g\bar{\mathbf{T}}_0 = \begin{bmatrix} \mathbf{\Lambda}_d & \mathbf{0} \\ \mathbf{0} & \hat{\mathbf{K}}_b \end{bmatrix}, \\ &\bar{\mathbf{u}}_p = \begin{bmatrix} \mathbf{q}_d \\ \mathbf{u}_b \end{bmatrix}, \quad \bar{\mathbf{f}}_p = \bar{\mathbf{T}}_0^T\begin{bmatrix} \mathbf{f}_s \\ \mathbf{f}_b \end{bmatrix}, \end{aligned} \tag{12}$$

in which the component matrices are defined by

$$\mathbf{I}_d = \mathbf{\Phi}_d^T\mathbf{M}_s\mathbf{\Phi}_d, \tag{13a}$$

$$\bar{\mathbf{M}}_c = \mathbf{\Phi}_d^T[\mathbf{M}_c - \mathbf{M}_s\mathbf{K}_s^{-1}\mathbf{K}_c], \tag{13b}$$

$$\hat{\mathbf{M}}_b = \mathbf{M}_b + \mathbf{K}_c^T\mathbf{K}_s^{-1}\mathbf{M}_s\mathbf{K}_s^{-1}\mathbf{K}_c - \mathbf{M}_c^T\mathbf{K}_s^{-1}\mathbf{K}_c - \mathbf{K}_c^T\mathbf{K}_s^{-1}\mathbf{M}_c, \tag{13c}$$

$$\mathbf{\Lambda}_d = \mathbf{\Phi}_d^T\mathbf{K}_s\mathbf{\Phi}_d, \tag{13d}$$

$$\hat{\mathbf{K}}_b = \mathbf{K}_b - \mathbf{K}_c^T\mathbf{K}_s^{-1}\mathbf{K}_c. \tag{13e}$$

From Eq. (12), the final reduced eigenvalue problem is obtained

$$\bar{\mathbf{K}}_p\bar{\mathbf{\Phi}}_p = \bar{\lambda}\bar{\mathbf{M}}_p\bar{\mathbf{\Phi}}_p \quad \text{with } \bar{\mathbf{u}}_p = \bar{\mathbf{\Phi}}_p\bar{\mathbf{q}}_p, \tag{14}$$

which is equivalent to Eq. (4). From Eqs. (11), (12) (13) (14), the approximated global eigenvector matrix $\bar{\mathbf{\Phi}}_g$ is defined by

$$\bar{\mathbf{\Phi}}_g = \bar{\mathbf{T}}_0\bar{\mathbf{\Phi}}_p. \tag{15}$$

3. Enhanced transformation matrix

As mentioned in the previous section, to construct the reduced transformation matrix $\bar{\mathbf{T}}_0$ in Eq. (11), the residual modes are truncated. However, when the residual terms are properly considered, the transformation matrix can be enhanced.

Using Eq. (10) in Eq. (8), $\mathbf{u}_g$ can be rewritten

$$\mathbf{u}_g = \begin{bmatrix} \mathbf{u}_s \\ \mathbf{u}_b \end{bmatrix} = \mathbf{T}_0 \begin{bmatrix} \mathbf{q}_d \\ \mathbf{q}_r \\ \mathbf{u}_b \end{bmatrix}, \quad \mathbf{T}_0 = \begin{bmatrix} \mathbf{\Phi}_d & \mathbf{\Phi}_r & -\mathbf{K}_s^{-1}\mathbf{K}_c \\ \mathbf{0} & \mathbf{0} & \mathbf{I}_b \end{bmatrix}. \tag{16}$$

Substituting Eq. (16) into Eq. (7), we obtain the equations of motion for the partitioned structure

$$\begin{aligned} &\left[\frac{d^2}{dt^2}\mathbf{M}_p + \mathbf{K}_p\right]\mathbf{u}_p = \mathbf{f}_p, \\ &\mathbf{M}_p = \mathbf{T}_0^T\mathbf{M}_g\mathbf{T}_0, \quad \mathbf{K}_p = \mathbf{T}_0^T\mathbf{K}_g\mathbf{T}_0, \\ &\frac{d^2}{dt^2}\mathbf{M}_p + \mathbf{K}_p = \begin{bmatrix} \hat{\mathbf{\Lambda}}_d & \mathbf{0} & \frac{d^2}{dt^2}\bar{\mathbf{M}}_c \\ \mathbf{0}^T & \hat{\mathbf{\Lambda}}_r & \frac{d^2}{dt^2}\mathbf{D} \\ \frac{d^2}{dt^2}\bar{\mathbf{M}}_c^T & \frac{d^2}{dt^2}\mathbf{D}^T & \hat{\mathbf{K}}_b + \frac{d^2}{dt^2}\hat{\mathbf{M}}_b \end{bmatrix}, \\ &\mathbf{u}_p = \begin{bmatrix} \mathbf{q}_d \\ \mathbf{q}_r \\ \mathbf{u}_b \end{bmatrix}, \quad \mathbf{f}_p = \mathbf{T}_0^T\begin{bmatrix} \mathbf{f}_s \\ \mathbf{f}_b \end{bmatrix}, \end{aligned} \tag{17}$$

where t denotes the time variable, and the component matrices are defined by

$$\hat{\mathbf{\Lambda}}_d = \mathbf{\Lambda}_d + \frac{d^2}{dt^2}\mathbf{I}_d, \tag{18a}$$

$$\hat{\mathbf{\Lambda}}_r = \mathbf{\Lambda}_r + \frac{d^2}{dt^2}\mathbf{I}_r, \quad \mathbf{\Lambda}_r = \mathbf{\Phi}_r^T\mathbf{K}_s\mathbf{\Phi}_r, \quad \mathbf{I}_r = \mathbf{\Phi}_r^T\mathbf{M}_s\mathbf{\Phi}_r, \tag{18b}$$

$$\mathbf{D} = \mathbf{\Phi}_r^T\left[-\mathbf{M}_s\mathbf{K}_s^{-1}\mathbf{K}_c + \mathbf{M}_c\right]. \tag{18c}$$

Note that Eq. (17) is the exact equations of motion that contains all of the substructural modes. Using the second row in Eq. (17) with $\mathbf{f}_p = \mathbf{0}$, we obtain

$$\mathbf{q}_r = -\hat{\mathbf{\Lambda}}_r^{-1}\left[\frac{d^2}{dt^2}\mathbf{D}\mathbf{u}_b\right]. \tag{19}$$

Using Eq. (19) in Eq. (16), $\mathbf{u}_s$ can be represented by

$$\mathbf{u}_s = \mathbf{\Phi}_d\mathbf{q}_d - \mathbf{K}_s^{-1}\mathbf{K}_c\mathbf{u}_b - \frac{d^2}{dt^2}\hat{\mathbf{F}}_r\left[-\mathbf{M}_s\mathbf{K}_s^{-1}\mathbf{K}_c + \mathbf{M}_c\right]\mathbf{u}_b, \tag{20}$$

with

$$\hat{\mathbf{F}}_r = \mathbf{\Phi}_r\hat{\mathbf{\Lambda}}_r^{-1}\mathbf{\Phi}_r^T = \mathbf{\Phi}_r\left[\mathbf{\Lambda}_r + \frac{d^2}{dt^2}\mathbf{I}_r\right]^{-1}\mathbf{\Phi}_r^T, \tag{21}$$

where $\hat{\mathbf{F}}_r$ represents the residual flexibility of the substructures.

We here invoke harmonic response ($d^2/dt^2 = -\omega^2$), and then $\hat{\mathbf{F}}_r$ can be approximated as

$$\begin{aligned} \hat{\mathbf{F}}_r &= \mathbf{\Phi}_r\left[\mathbf{\Lambda}_r - \omega^2\mathbf{I}_r\right]^{-1}\mathbf{\Phi}_r^T \\ &\approx \mathbf{\Phi}_r\mathbf{\Lambda}_r^{-1}\mathbf{\Phi}_r^T + \omega^2\mathbf{\Phi}_r\mathbf{\Lambda}_r^{-2}\mathbf{\Phi}_r^T = \mathbf{F}_{rs} + \omega^2\mathbf{F}_{rm}, \end{aligned} \tag{22}$$

where $\mathbf{F}_{rs}$ and $\mathbf{F}_{rm}$ mean the static and dynamic parts of the residual flexibilities, respectively.

Using Eq. (22) in Eq. (20) and truncating terms higher than order of ω^2, $\mathbf{u}_s$ can be approximated

$$\mathbf{u}_s \approx \bar{\mathbf{u}}_s = \mathbf{\Phi}_d\mathbf{q}_d - \mathbf{K}_s^{-1}\mathbf{K}_c\mathbf{u}_b + \omega^2\mathbf{F}_{rs}\left[-\mathbf{M}_s\mathbf{K}_s^{-1}\mathbf{K}_c + \mathbf{M}_c\right]\mathbf{u}_b, \tag{23}$$

and $\mathbf{F}_{rs}$ is indirectly calculated using the full and dominant flexibilities as

$$\mathbf{F}_{rs} = \mathbf{K}_s^{-1} - \mathbf{\Phi}_d\mathbf{\Lambda}_d^{-1}\mathbf{\Phi}_d^T. \tag{24}$$

Using Eqs. (23) and (24) in Eq. (8), we finally have

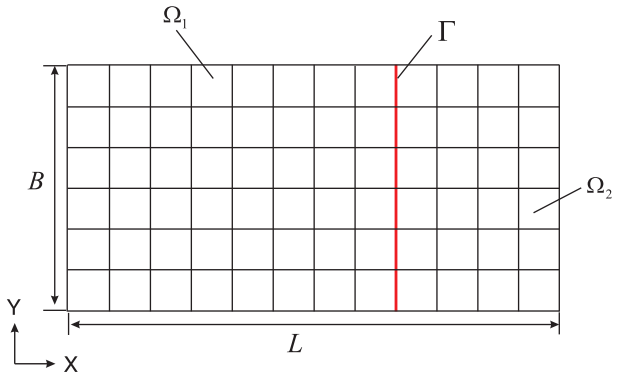

Fig. 2. Rectangular plate problem ($L = 0.6096$ m, $B = 0.3048$ m, $h = 3.175\times 10^{-3}$ m, $E = 72$ GPa, $\nu = 0.33$ and $\rho_s = 2796$ kg/m^3).

Table 1
Retained substructural mode numbers $N_d^{(k)}$ in the rectangular plate problem.

Mode selection method	Case	$N_d^{(1)}$	$N_d^{(2)}$	N_d
Freq. cut-off	1	10	5	15
	2	21	9	30
Kim and Lee [18]	1	10	5	15
	2	21	9	30

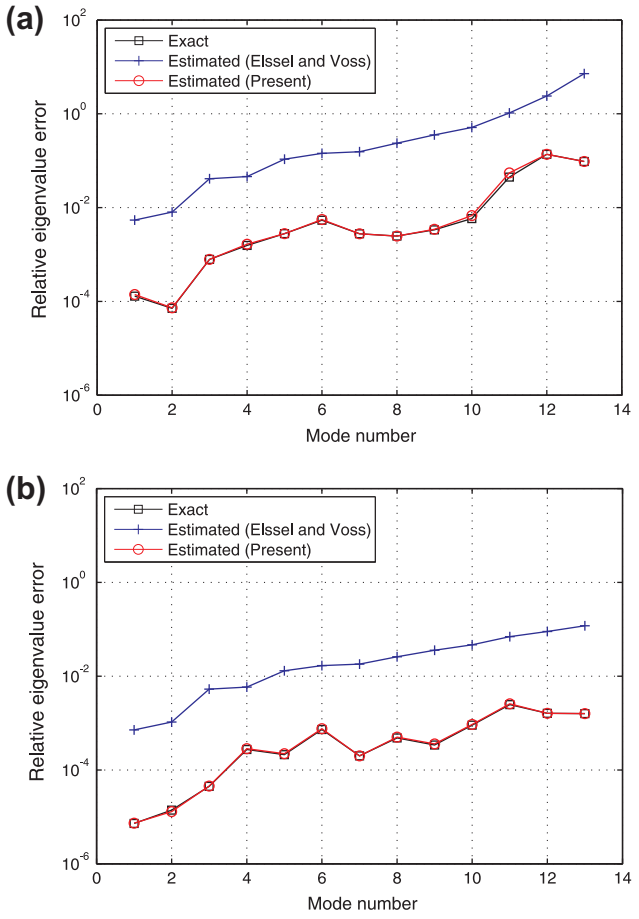

Fig. 3. Exact and estimated relative eigenvalue errors in the rectangular plate problem. The frequency cut-off mode selection method is used. (a) $N_d = 15$, (b) $N_d = 30$.

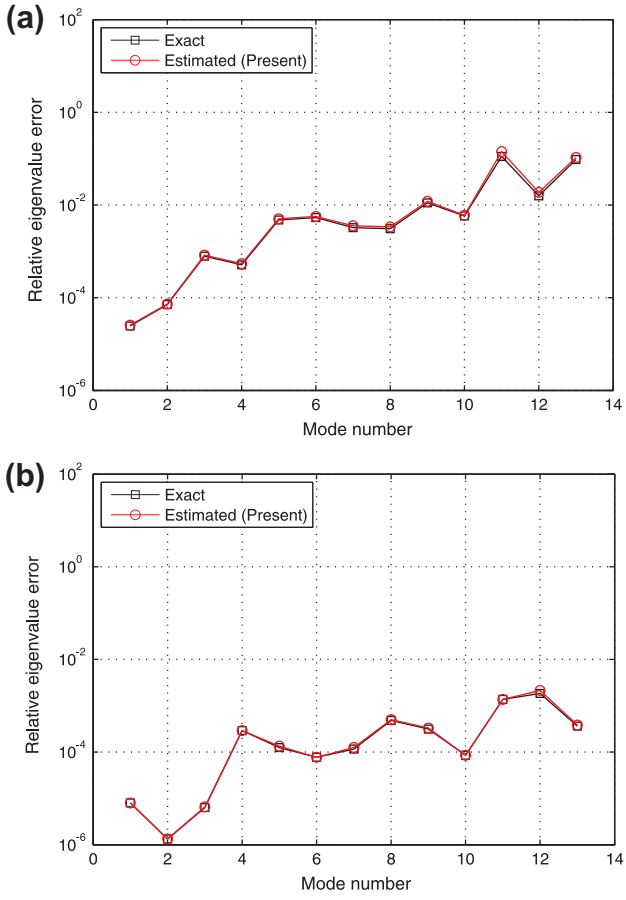

Fig. 4. Exact and estimated relative eigenvalue errors in the rectangular plate problem. The mode selection method proposed by Kim and Lee [18] is used. (a) $N_d = 15$, $\tilde{N}_d = 30$, (b) $N_d = 30$, $\tilde{N}_d = 60$. Here, $\tilde{N}_d$ is the total number of the retained modes for the intermediate eigenvalue problem.

$$\mathbf{u}_g \approx \bar{\mathbf{u}}_g = \bar{\mathbf{T}}_1 \begin{bmatrix} \mathbf{q}_d \\ \mathbf{u}_b \end{bmatrix}, \quad \bar{\mathbf{T}}_1 = \bar{\mathbf{T}}_0 + \bar{\mathbf{T}}_r, \tag{25}$$

with

$$\bar{\mathbf{T}}_r = \begin{bmatrix} \mathbf{0} & \omega^2 \mathbf{F}_{rs}\left[-\mathbf{M}_s\mathbf{K}_s^{-1}\mathbf{K}_c + \mathbf{M}_c\right] \\ \mathbf{0} & \mathbf{0} \end{bmatrix}, \tag{26}$$

where $\bar{\mathbf{T}}_1$ is the transformation matrix enhanced by $\bar{\mathbf{T}}_r$. Therefore, using $\bar{\mathbf{T}}_1$, the approximated global displacement vector $\bar{\mathbf{u}}_g$ can be more accurately defined, and then the approximated global eigenvector matrix $\bar{\mathbf{\Phi}}_g$ can be also enhanced as follows:

Table 2
Exact and estimated eigenvalue errors in the rectangular plate problem (The frequency cut-off mode selection method is used and $N_d = 15$).

Mode number	Exact	Estimated (Elssel and Voss)	Estimated (Present)
1	1.29749E−04	5.40922E−03	1.39749E−04
2	7.11199E−05	8.03123E−03	7.31199E−05
3	7.87912E−04	4.13343E−02	7.87912E−04
4	1.55629E−03	4.60452E−02	1.65629E−03
5	2.78188E−03	1.07879E−01	2.78188E−03
6	5.38288E−03	1.43772E−01	5.58288E−03
7	2.75964E−03	1.55603E−01	2.76964E−03
8	2.46485E−03	2.36205E−01	2.46485E−03
9	3.35683E−03	3.53565E−01	3.45683E−03
10	5.82414E−03	5.09857E−01	6.74143E−03
11	4.48544E−02	1.04450E+00	5.48544E−02
12	1.36776E−01	2.40284E+00	1.36776E−01
13	9.63322E−02	7.17569E+00	9.63322E−02

$$\bar{\Phi}_g = \bar{\mathbf{T}}_1 \bar{\Phi}_p. \tag{27}$$

To construct the enhanced transformation matrix $\bar{\mathbf{T}}_1$, the residual flexibility $\mathbf{F}_{rs}$ is additionally calculated. However, $\mathbf{F}_{rs}$ is simply calculated by reusing $\mathbf{K}_s^{-1}$ and dominant substructural eigensolutions (see Eq. (24)).

4. Error estimator

In CMS methods, the following relative eigenvalue error is generally used to evaluate the reliability of the reduced model

$$\xi_i = \frac{\bar{\lambda}_i - \lambda_i}{\lambda_i}, \tag{28}$$

in which ξ_i denotes the relative eigenvalue error for the ith mode and the exact global eigenvalue λ_i is obtained from the global (original) eigenvalue problem.

We here derive an error estimator to precisely evaluate the relative eigenvalue error in the CB method without knowing the exact global eigenvalue λ_i.

The exact global eigensolutions are expressed by the approximated global eigensolutions and their error terms as

$$\lambda_i = \bar{\lambda}_i + \delta\lambda_i, \tag{29a}$$

$$(\boldsymbol{\phi}_g)_i = (\bar{\boldsymbol{\phi}}_g)_i + (\delta\boldsymbol{\phi}_g)_i, \tag{29b}$$

where $\delta\lambda_i$ and $(\delta\boldsymbol{\phi}_g)_i$ are errors in the ith eigenvalue and eigenvector, respectively.

Due to the linear independency of the exact global eigenvectors, the approximated global eigenvector $(\bar{\boldsymbol{\phi}}_g)_i$ can be represented by a linear combination of the exact global eigenvectors

$$(\bar{\boldsymbol{\phi}}_g)_i = \sum_{k=1}^{N_g} \alpha_k (\boldsymbol{\phi}_g)_k, \tag{30}$$

where α_k are coefficients for the linear combination.

As more substructural modes are contained in the reduced model, the approximated global eigenvector $(\bar{\boldsymbol{\phi}}_g)_i$ calculated from the reduced eigenvalue problem becomes closer to the exact global eigenvector $(\boldsymbol{\phi}_g)_i$. When the approximated global eigenvectors are close enough to the exact global eigenvector, we can assume

$$\alpha_i \approx 1, \tag{31a}$$

$$|\,\alpha_i\,| \gg |\,\alpha_i - 1\,|, \quad |\,\alpha_1\,|, \quad |\,\alpha_2\,|, \ldots |\,\alpha_{i-1}\,|, \quad |\,\alpha_{i+1}\,|, \ldots, |\,\alpha_{N_g}\,|\,. \tag{31b}$$

Since the exact eigensolutions $(\lambda_i, (\boldsymbol{\phi}_g)_i)$ are obtained from the global eigenvalue problem in Eq. (2), the following equation is given:

$$\frac{1}{\lambda_i}(\boldsymbol{\phi}_g)_i^T \mathbf{K}_g (\boldsymbol{\phi}_g)_i = (\boldsymbol{\phi}_g)_i^T \mathbf{M}_g (\boldsymbol{\phi}_g)_i. \tag{32}$$

The global eigensolutions λ_i and $(\boldsymbol{\phi}_g)_i$ satisfy the mass-orthonormality and stiffness-orthogonality conditions in Eqs. (3a) and (3b), respectively. Using Eq. (29b) in Eq. (32), we obtain

$$\frac{1}{\lambda_i}\left[(\bar{\boldsymbol{\phi}}_g)_i + (\delta\boldsymbol{\phi}_g)_i\right]^T \mathbf{K}_g \left[(\bar{\boldsymbol{\phi}}_g)_i + (\delta\boldsymbol{\phi}_g)_i\right] = \left[(\bar{\boldsymbol{\phi}}_g)_i + (\delta\boldsymbol{\phi}_g)_i\right]^T \mathbf{M}_g \left[(\bar{\boldsymbol{\phi}}_g)_i + (\delta\boldsymbol{\phi}_g)_i\right]. \tag{33}$$

Table 3
Retained substructural mode numbers $N_d^{(k)}$ in the shaft–shaft interaction problem.

Mode selection method	Case	$N_d^{(1)}$	$N_d^{(2)}$	N_d
Freq. cut-off	1	13	7	20
	2	24	16	40
Kim and Lee [18]	1	13	7	20
	2	26	14	40

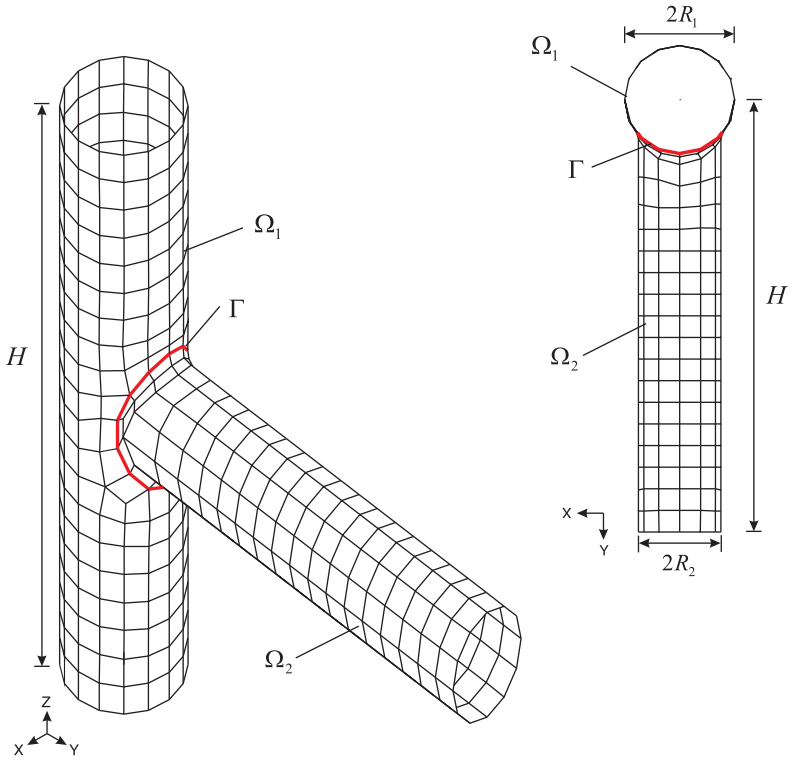

Fig. 5. Shaft–shaft interaction problem ($H = 0.08$ m, $h = 0.5 \times 10^{-3}$ m, $R_1 = 0.01$ m, $R_2 = 0.0075$ m, $E = 207$ GPa, $\nu = 0.29$ and $\rho_s = 2700$ kg/m^3).

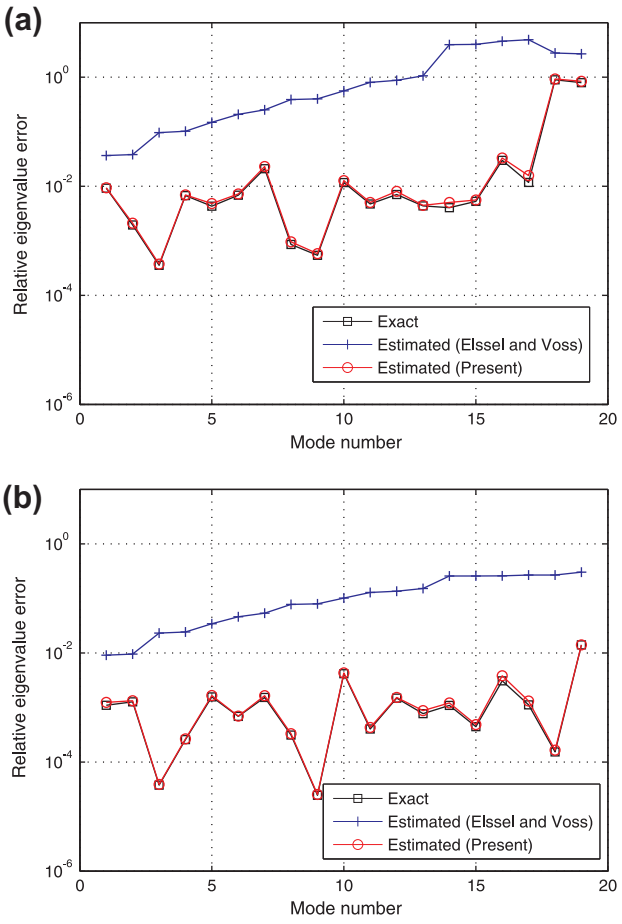

Fig. 6. Exact and estimated relative eigenvalue errors in the shaft–shaft interaction problem. The frequency cut-off mode selection method is used. (a) $N_d = 20$, (b) $N_d = 40$.

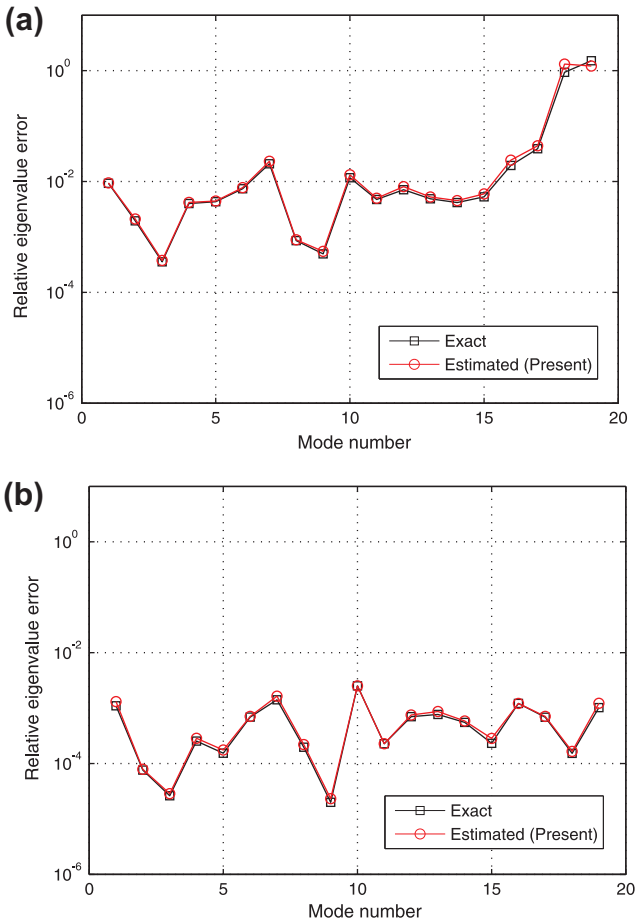

Fig. 7. Exact and estimated relative eigenvalue errors in the shaft–shaft interaction problem. The mode selection method proposed by Kim and Lee [18] is used. (a) $N_d = 20$, $\tilde{N}_d = 40$, (b) $N_d = 40$, $\tilde{N}_d = 80$. Here, $\tilde{N}_d$ is the total number of the retained modes for the intermediate eigenvalue problem.

Using Eq. (30) in Eq. (33), the left-hand side of Eq. (33) can be rewritten as follows:

$$\frac{1}{\lambda_i}\left[(\bar{\phi}_g)_i + (\delta\phi_g)_i\right]^T \mathbf{K}_g \left[(\bar{\phi}_g)_i + (\delta\phi_g)_i\right] = \frac{1}{\lambda_i}(\bar{\phi}_g)_i^T \mathbf{K}_g (\bar{\phi}_g)_i - 2(\alpha_i - 1) - \left[(\alpha_i - 1)^2 + \sum_{\substack{k=1 \\ k\neq i}}^{N_g} \alpha_k^2 \frac{\lambda_k}{\lambda_i}\right]. \tag{34}$$

Similarly, the right-hand side of Eq. (33) also becomes

$$\left[(\bar{\phi}_g)_i + (\delta\phi_g)_i\right]^T \mathbf{M}_g \left[(\bar{\phi}_g)_i + (\delta\phi_g)_i\right] = (\bar{\phi}_g)_i^T \mathbf{M}_g (\bar{\phi}_g)_i - 2(\alpha_i - 1) - \left[(\alpha_i - 1)^2 + \sum_{\substack{k=1 \\ k\neq i}}^{N_g} \alpha_k^2\right]. \tag{35}$$

Using Eqs. (34) and (35) in Eq. (33), the leading order terms $2(\alpha_i - 1)$ are canceled, and the following equation is obtained:

$$\frac{1}{\lambda_i}(\bar{\phi}_g)_i^T \mathbf{K}_g (\bar{\phi}_g)_i - (\bar{\phi}_g)_i^T \mathbf{M}_g (\bar{\phi}_g)_i - \sum_{\substack{k=1 \\ k\neq i}}^{N_g} \alpha_k^2 \left(\frac{\lambda_k}{\lambda_i} - 1\right) = 0. \tag{36}$$

In the CB method, using the enhanced transformation matrix $\bar{\mathbf{T}}_1$ in Eq. (27), the approximated global eigenvector $(\bar{\phi}_g)_i$ can be defined

$$(\bar{\phi}_g)_i = \bar{\mathbf{T}}_1 (\bar{\phi}_p)_i \quad \text{with } \bar{\mathbf{T}}_1 = \bar{\mathbf{T}}_0 + \bar{\mathbf{T}}_r. \tag{37}$$

Using Eq. (37), Eq. (36) is rewritten by

$$\frac{1}{\lambda_i}(\bar{\phi}_p)_i^T \left[\bar{\mathbf{T}}_0 + \bar{\mathbf{T}}_r\right]^T \mathbf{K}_g \left[\bar{\mathbf{T}}_0 + \bar{\mathbf{T}}_r\right](\bar{\phi}_p)_i - (\bar{\phi}_p)_i^T \left[\bar{\mathbf{T}}_0 + \bar{\mathbf{T}}_r\right]^T \mathbf{M}_g \left[\bar{\mathbf{T}}_0 + \bar{\mathbf{T}}_r\right](\bar{\phi}_p)_i - \sum_{\substack{k=1 \\ k\neq i}}^{N_g} \alpha_k^2 \left(\frac{\lambda_k}{\lambda_i} - 1\right) = 0. \tag{38}$$

After expanding Eq. (38) and using the mass-orthonormality and stiffness-orthogonality in Eq. (5), we obtain

$$\frac{\bar{\lambda}_i}{\lambda_i} - 1 = 2(\bar{\phi}_p)_i^T \bar{\mathbf{T}}_0^T \left[\mathbf{M}_g - \frac{1}{\lambda_i}\mathbf{K}_g\right] \bar{\mathbf{T}}_r (\bar{\phi}_p)_i + (\bar{\phi}_p)_i^T \bar{\mathbf{T}}_r^T \left[\mathbf{M}_g - \frac{1}{\lambda_i}\mathbf{K}_g\right] \bar{\mathbf{T}}_r (\bar{\phi}_p)_i + \sum_{\substack{k=1 \\ k\neq i}}^{N_g} \alpha_k^2 \left(\frac{\lambda_k}{\lambda_i} - 1\right), \tag{39}$$

where the left-hand side is the relative eigenvalue error. Therefore, Eq. (39) shows that the relative eigenvalue error can be expressed by three scalar terms.

The last term on the right-hand side of Eq. (39) is much smaller than the other terms due to α_k^2 under the assumption in Eq. (31). Neglecting the last term, we obtain

$$\frac{\bar{\lambda}_i}{\lambda_i} - 1 \approx 2(\bar{\phi}_p)_i^T \bar{\mathbf{T}}_0^T \left[\mathbf{M}_g - \frac{1}{\lambda_i}\mathbf{K}_g\right] \bar{\mathbf{T}}_r (\bar{\phi}_p)_i + (\bar{\phi}_p)_i^T \bar{\mathbf{T}}_r^T \left[\mathbf{M}_g - \frac{1}{\lambda_i}\mathbf{K}_g\right] \bar{\mathbf{T}}_r (\bar{\phi}_p)_i, \tag{40}$$

which can be used to estimate the relative eigenvalue error.

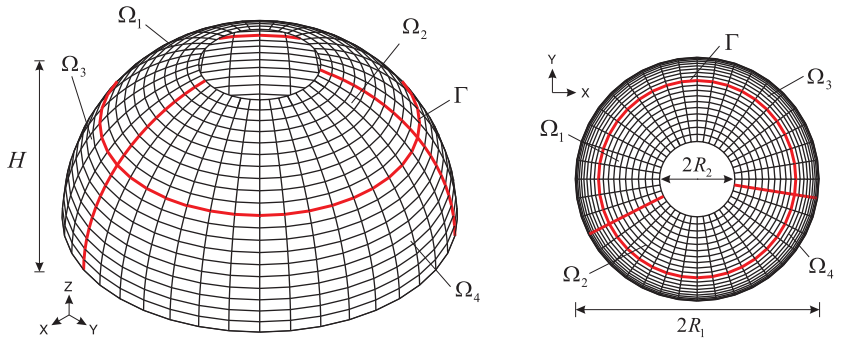

Fig. 8. Hemisphere shell problem ($H = 3.804$ m, $R_1 = 2$ m, $R_2 = 0.618$ m, $h = 0.05$ m, $E = 69$ GPa, $\nu = 0.35$ and $\rho_s = 2700$ kg/m^3).

Table 4
Retained substructural mode numbers $N_d^{(k)}$ in the hemisphere shell problem.

Mode selection method	Case	$N_d^{(1)}$	$N_d^{(2)}$	$N_d^{(3)}$	$N_d^{(4)}$	N_d
Freq. cut-off	1	3	2	12	8	25
	2	17	10	32	21	80
Kim and Lee [18]	1	2	2	13	8	25
	2	16	10	33	21	80

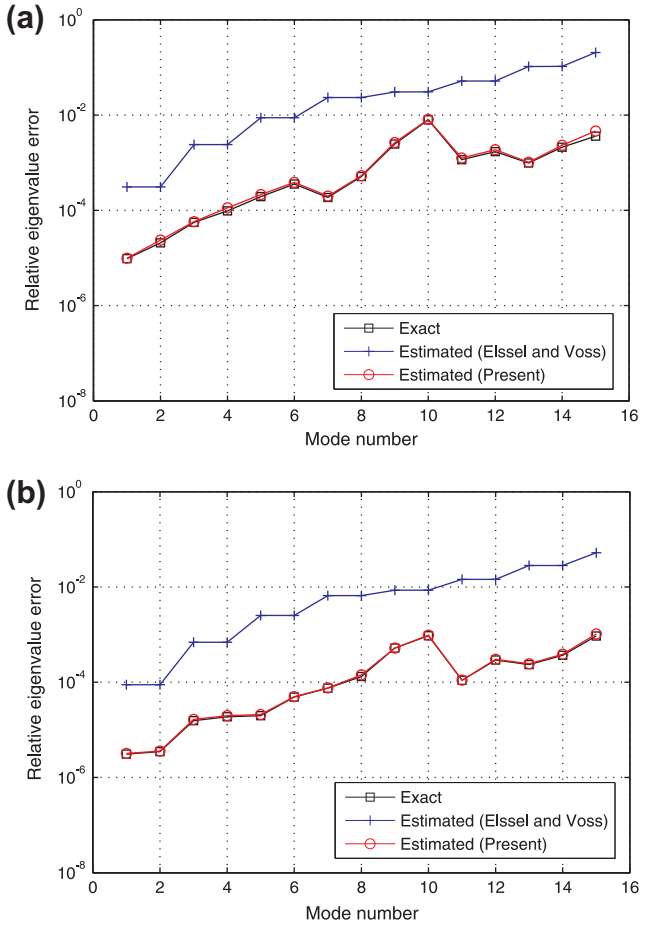

Fig. 9. Exact and estimated relative eigenvalue errors in the hemisphere shell problem. The frequency cut-off mode selection method is used. (a) $N_d = 25$, (b) $N_d = 80$.

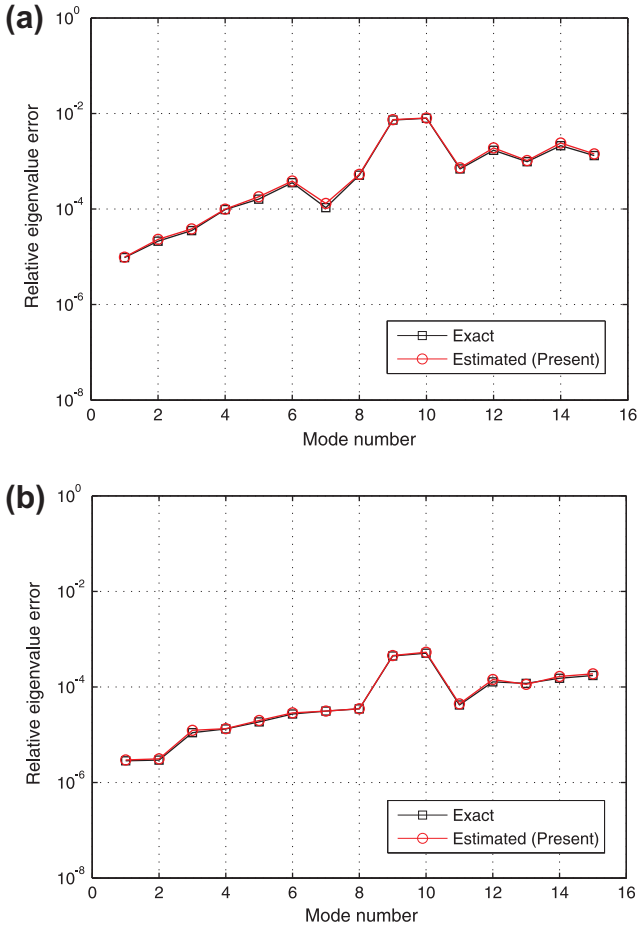

Fig. 10. Exact and estimated relative eigenvalue errors in the hemisphere shell problem. The mode selection method proposed by Kim and Lee [18] is used. (a) $N_d = 25$, $\tilde{N}_d = 50$, (b) $N_d = 80$, $\tilde{N}_d = 160$. Here, $\tilde{N}_d$ is the total number of the retained modes for the intermediate eigenvalue problem.

Finally, let us define the error estimator η_i as

$$\eta_i = 2(\bar{\boldsymbol{\phi}}_p)_i^T \bar{\mathbf{T}}_0^T \left[\mathbf{M}_g - \frac{1}{\bar{\lambda}_i}\mathbf{K}_g\right] \bar{\mathbf{T}}_r (\bar{\boldsymbol{\phi}}_p)_i + (\bar{\boldsymbol{\phi}}_p)_i^T \bar{\mathbf{T}}_r^T \left[\mathbf{M}_g - \frac{1}{\bar{\lambda}_i}\mathbf{K}_g\right] \bar{\mathbf{T}}_r (\bar{\boldsymbol{\phi}}_p)_i, \tag{41}$$

with

$$\bar{\mathbf{T}}_r = \bar{\lambda}_i \begin{bmatrix} \mathbf{0} & \mathbf{F}_{rs}\left[-\mathbf{M}_s\mathbf{K}_s^{-1}\mathbf{K}_c + \mathbf{M}_c\right] \\ \mathbf{0} & \mathbf{0} \end{bmatrix}. \tag{42}$$

It is very important that, for λ_i in Eq. (40) and ω^2 contained in $\bar{\mathbf{T}}_r$ in Eq. (26), the ith approximated eigenvalue $\bar{\lambda}_i$ calculated from the reduced eigenvalue problem is used to calculate η_i. However, the enhanced transformation matrix $\bar{\mathbf{T}}_1$ cannot be used to improve the CB method in its present form because ω^2 in the transformation matrix is unknown. Therefore, the enhanced transformation matrix $\bar{\mathbf{T}}_1$ is only used for error estimation.

We note that, for higher modes, the assumption in Eq. (31) could not be well satisfied and $\lambda_k/\lambda_i - 1$ could increase, in particular, when selected dominant modes are not many enough. Therefore, the proposed error estimator will give better accuracy for lower modes in general. It is also valuable to note that the computational cost of the error estimator proposed is not high because simple matrix additions and multiplications are required in Eqs. (41) and (42).

5. Numerical examples

In this section, we test the performance of the proposed error estimator. Four different structural problems are considered: rectangular plate, shaft–shaft interaction, hemisphere shell, and stiffened plate problems.

The conventional frequency cut-off mode selection method and recently developed mode selection method [18] are employed to select the dominant substructural modes.

When the frequency cut-off mode selection method is used, the performance of the present error estimator is compared with the previous one developed by Elssel and Voss [16]

$$\eta_i' = \frac{\bar{\lambda}_i}{|\lambda_r - \bar{\lambda}_i|}, \tag{43}$$

where λ_r is the smallest residual eigenvalue of substructures. The error estimator η_i' was proposed as an upper bound of the relative eigenvalue error

$$0 \leqslant \xi_i \leqslant \eta_i'. \tag{44}$$

Note that almost no computational cost is required for evaluating this error estimator.

The mode selection method developed by Kim and Lee [18] uses the eigenvector relation between substructures and global structure. Since this mode selection method can rank the substructural modal contributions to the global modes, it can improve the solution accuracy compared to the frequency cut-off mode selection method. The proposed error estimator is also tested using this new mode selection method.

Table 5
Retained substructural mode numbers $N_d^{(k)}$ in the stiffened plate problem.

Mode selection method	Case	$N_d^{(1)}$	$N_d^{(2)}$	$N_d^{(3)}$	$N_d^{(4)}$	$N_d^{(5)}$	$N_d^{(6)}$	N_d
Freq. cut-off	1	11	4	1	1	4	4	25
	2	27	16	6	6	10	10	75
Kim and Lee [18]	1	9	3	2	1	5	5	25
	2	22	15	8	8	11	11	75

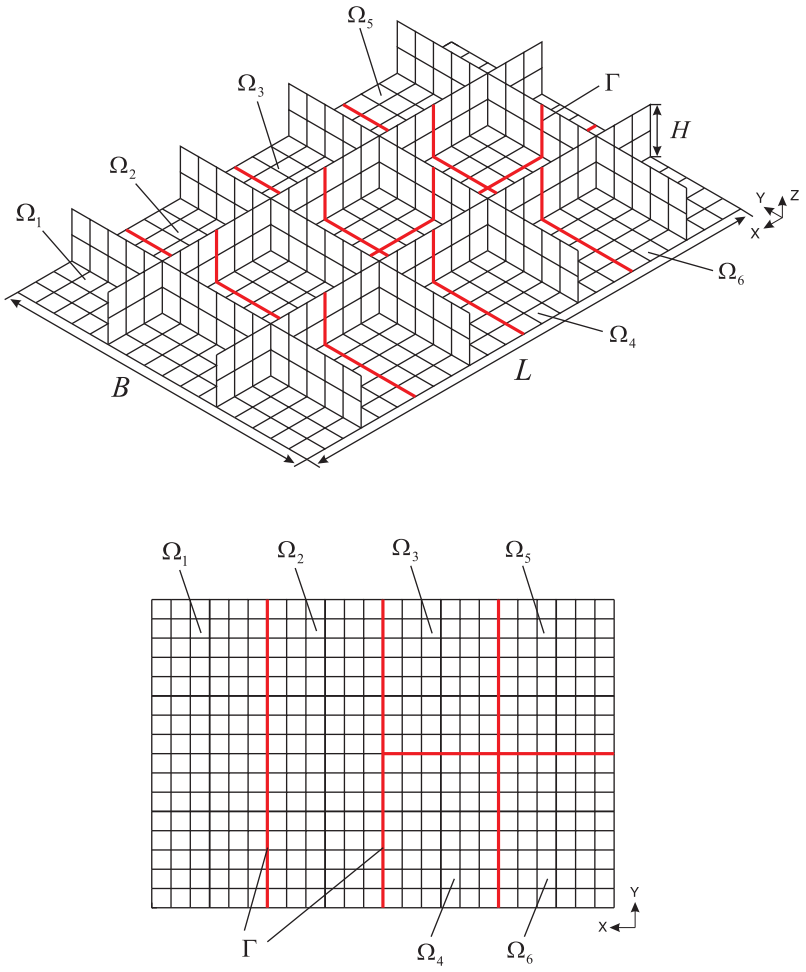

Fig. 11. Stiffened plate problem ($L = 4.8$ m, $B = 3.2$ m, $H = 0.5$ m, $h = 0.03$ m, $E = 210$ GPa, $\nu = 0.30$ and $\rho_s = 7850$ kg/m^3).

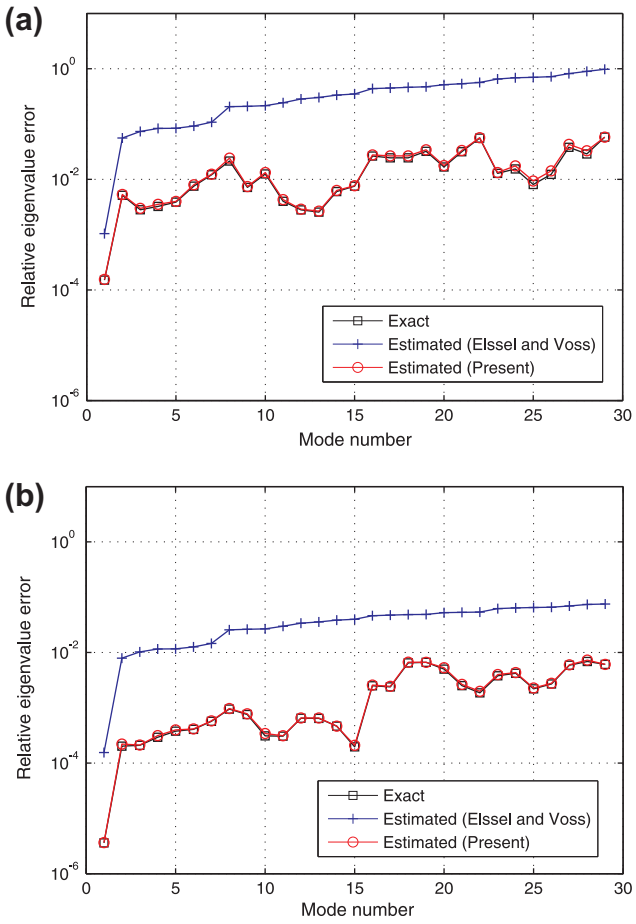

Fig. 12. Exact and estimated relative eigenvalue errors in the stiffened plate problem. The frequency cut-off mode selection method is used. (a) $N_d = 25$, (b) $N_d = 75$.

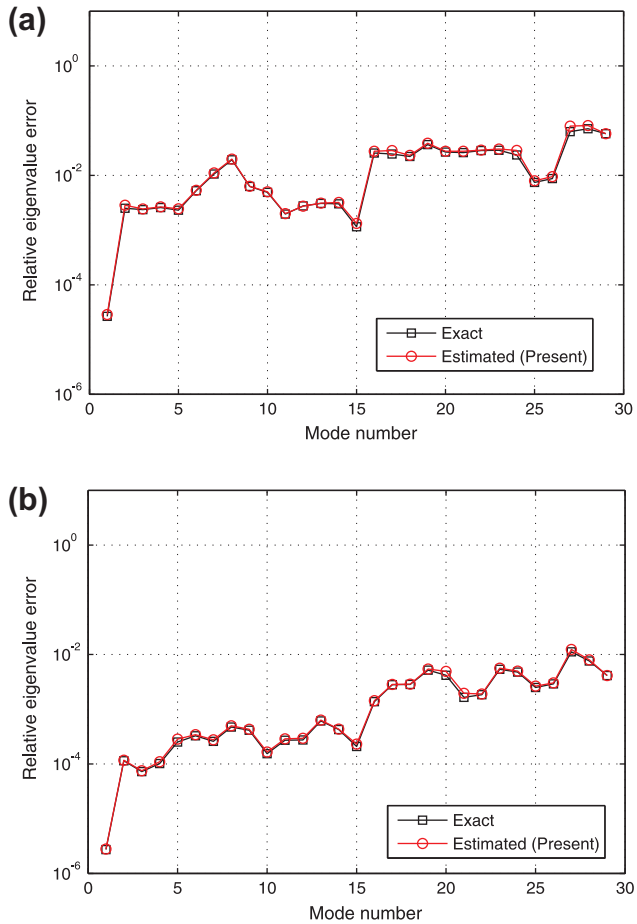

Fig. 13. Exact and estimated relative eigenvalue errors in the stiffened plate problem. The mode selection method proposed by Kim and Lee [18] is used. (a) $N_d = 25,\ \widetilde{N}_d = 50$, (b) $N_d = 75,\ \widetilde{N}_d = 150$. Here, $\widetilde{N}_d$ is the total number of the retained modes for the intermediate eigenvalue problem.

The 4-node MITC shell finite elements developed by Dvorkin and Bathe [19] is used for the finite element modeling. The MITC shell finite element is a well-known shell finite element that can effectively alleviate shear locking (see, e.g., Refs. [19–24]).

5.1. Rectangular plate problem

Let us consider a rectangular plate with free boundary, see Fig. 2. Length L is 0.6096 m, width B is 0.3048 m, and thickness h is 3.175×10^{-3} m. Young's modulus E is 72 GPa, Poisson's ratio ν is 0.33, and density ρ_s is 2796 kg/m^3. The plate is modeled by a 12×6 mesh of the 4-node MITC shell finite elements and the structural model is partitioned into two substructures ($N_s = 2$).

Here, 15 and 30 substructural modes are retained for two numerical cases ($N_d = 15,\ N_d = 30$), and the numbers of retained substructural modes are listed in Table 1. Figs. 3 and 4 present the exact and estimated relative eigenvalue errors, respectively. Fig. 3 shows that the present error estimator outperforms the error estimator by Elssel and Voss [16] when the frequency cut-off mode selection method is used. Fig. 4 also shows the excellent performance of the present error estimator when the mode selection method by Kim and Lee [18] is used. In Table 2, we list the exact and estimated relative eigenvalue errors corresponding to Fig. 3(a).

5.2. Shaft–shaft interaction problem

We here consider two cylindrical shafts connected with fillets of radius 0.002 m and no boundary condition is imposed, see Fig. 5 [23]. Height H is 0.08 m, and thickness h is 0.5×10^{-3} m. The radii R_1 and R_2 are 0.01 m and 0.0075 m, respectively. Young's modulus E is 207 GPa, Poisson's ratio ν is 0.29, and density ρ_s is 2700 kg/m^3. For this example, 534 elements and 555 nodes are used, and the finite element model is partitioned into two substructures ($N_s = 2$).

Two different numbers of retained substructural modes ($N_d = 20,\ N_d = 40$) are considered as listed in Table 3. Figs. 6 and 7 show the excellent performance of the present error estimator, which also shows much better accuracy than the previous error estimator by Elssel and Voss [16].

5.3. Hemisphere shell problem

Let us consider a hemisphere shell structure with free boundary at both ends, see Fig. 8. Height H is 3.084 m, and thickness h is 0.05 m. The radii R_1 and R_2 are 2 m and 0.618 m, respectively. Young's modulus E is 69 GPa, Poisson's ratio ν is 0.35, and density ρ_s is 2700 kg/m^3. In this problem, 20 and 40 shell finite elements are used in the axial and circumferential directions, respectively. The hemisphere shell is partitioned into four substructures ($N_s = 4$).

We consider 25 and 80 substructural modes ($N_d = 25,\ N_d = 80$), see Table 4. As shown in Figs. 9 and 10, the present error estimator very accurately estimates the relative eigenvalue errors in the two numerical cases.

Table 6
Computation times for the exact and estimated relative eigenvalue errors.

	DOFs		Computation time (sec)		
	N_g	$\overline{N}_p$	Exact	Estimated using Eq. (43) (Elssel and Voss)	Estimated using Eq. (41) (Present)
Rectangular plate (Freq. cut-off, $N_d = 15$)	273	36	2.160E−01	1.548E−05	1.936E−03
Shaft–shaft interaction (Freq. cut-off, $N_d = 20$)	2775	90	3.735E+00	1.897E−05	2.186E−02
Hemisphere shell (Freq. cut-off, $N_d = 25$)	4200	425	1.722E+01	3.597E−05	4.722E−02
Stiffened plate (Freq. cut-off, $N_d = 25$)	3351	423	5.141E+00	9.131E−06	2.413E−02

5.4. Stiffened plate problem

We here apply the present error estimator to a stiffened plate with free boundary, see Fig. 11. Length L is 4.8 m, width B is 3.2 m, and thickness h is 0.03 m. The flat plate has two longitudinal and four transverse stiffeners, and height H is 0.5 m. Young's modulus E is 210 GPa, Poisson's ratio ν is 0.3, and density ρ_s is 7850 kg/m^3. The bottom plate is modeled by 24×16 shell finite elements, and the longitudinal and transverse stiffeners are modeled by 24×2 and 16×2 shell finite elements, respectively. This stiffened plate is partitioned into six substructures ($N_s = 6$).

We use 25 and 75 substructural modes ($N_d = 25,\ N_d = 75$) in two numerical cases, and the numbers of dominant substructural modes $N_d^{(k)}$ are listed in Table 5. The exact and estimated eigenvalue errors are plotted in Figs. 12 and 13, and the graphs clearly show the robustness of the present error estimator.

5.5. Computational cost

In order to investigate the computational cost required for the error estimator proposed, computation times are measured for the exact and estimated relative eigenvalue errors. MATLAB is used for the computation with a personal computer (Intel duo-core E6750, 2.66 GHz CPU, 8.0 GB RAM).

Table 6 presents the computation times for the relative eigenvalue errors in the four numerical examples, in which the computations are performed only for the lowest eigenvalues (mode number = 1). Note that, for the exact relative eigenvalue error, we consider the solution time of the exact lowest eigenvalue using Eq. (1) and the calculation time of the exact relative eigenvalue error using Eq. (28). The results show that the proposed error estimator is computationally efficient.

6. Conclusions

In this paper, we have proposed an error estimator to accurately estimate the relative eigenvalue errors in the CB method. To develop the error estimator, we here propose an enhanced transformation matrix considering the residual mode effects that are truncated in the original CB formulation. Due to the compensation of the residual modes, the original transformation matrix can be enhanced, and then the global eigenvectors can be approximated more accurately than the original transformation matrix. Using the enhanced transformation matrix, we can derive an error estimator for the CB method from the global eigenvalue problem.

Through various numerical tests, we presented the excellent performance of the error estimator proposed in this study. Although the present error estimator requires an enhanced transformation matrix, the required matrix operations are simply additions and multiplications of known matrices. For this reason, the present error estimator possesses not only improved accuracy but also computational efficiency.

The error estimator proposed in this study would be used to develop the mode selection algorithms for the reduced-order modeling and the solution techniques for eigenvalue problems in structural dynamics.

Acknowledgements

This work was supported by the Human Resources Development program (No. 20114030200040) of the Korea Institute of Energy Technology Evaluation and Planning (KETEP) grant funded by the Korea government Ministry of Trade, Industry and Energy.

References

[1] Craig RR, Bampton MCC. Coupling of substructures for dynamic analysis. AIAA J 1968;6(7):1313–9.
[2] Hurty W. Dynamic analysis of structural systems using component modes. AIAA J 1965;3(4):678–85.
[3] Guyan R. Reduction of stiffness and mass matrices. AIAA J 1965;3(2):380.
[4] MacNeal RH. Hybrid method of component mode synthesis. Comput Struct 1971;1(4):581–601.
[5] Benfield WA, Hruda RF. Vibration analysis of structures by component mode substitution. AIAA J 1971;9:1255–61.
[6] Rubin S. Improved component-mode representation for structural dynamic analysis. AIAA J 1975;13(8):995–1006.
[7] Hintz RM. Analytical methods in component modal synthesis. AIAA J 1975;13(8):1007–16.
[8] Bennighof JK, Lehoucq RB. An automated multilevel substructuring method for eigenspace computation in linear elastodynamics. SIAM J Sci Comput 2004;25:2084106.
[9] Park KC, Park YH. Partitioned component mode synthesis via a flexibility approach. AIAA J 2004;42(6):1236–45.
[10] Rixen DJ. A dual Craig-Bampton method for dynamic substructuring. J Comput Appl Math 2004;168(1–2):383–91.
[11] Markovic D, Park KC, Ibrahimbegovic A. Reduction of substructural interface degrees of freedom in flexibility-based component mode synthesis. Int J Numer Methods Eng 2007;70:163–80.
[12] Klerk DD, Rixen DJ, Voormeeren SN. General framework for dynamic substructuring: history, review, and classification of techniques. AIAA J 2008;46(5):1169–81.
[13] Park KC, Kim JG, Lee PS. A mode selection criterion based on flexibility approach in component mode synthesis. In: Proceeding 53rd AIAA/ASME/ASCE/AHS/ASC structures, structural dynamics, and materials conference USA. Hawaii; 2012.
[14] Bourquin F. Analysis and comparison of several component mode synthesis methods on one dimensional domains. Numer Math 1990;58(1):11–33.
[15] Yang C, Gao W, Bai Z, Li XS, Lee LQ, Husbands P, et al. An algebraic substructuring method for large-scale eigenvalue calculation. SIAM J Sci Comput 2005;27:873–92.
[16] Elssel K, Voss H. An a priori bound for automated multilevel substructuring. SIAM J Matrix Anal Appl 2007;28(2):386–97.
[17] Jakobsson H, Larson MG. A posteriori error analysis of component mode synthesis for the elliptic eigenvalue problem. Comput Methods Appl Mech Eng 2011;200:2840–7.

[18] Kim JG, Lee PS. Mode selection and error estimation methods for the flexibility based component mode synthesis method. In: OSE (Ocean Systems Engineering) REPORT, 2013.
[19] Dvorkin EN, Bathe KJ. A continuum mechanics based four-node shell element for general nonlinear analysis. Eng Comput 1984;1:77–88.
[20] Bathe KJ, Dvorkin EN. A formulation of general shell elements the use of mixed interpolation of tensorial components. Int J Numer Methods Eng 1986;22:697–722.
[21] Lee PS, Bathe KJ. Development of MITC isotropic triangular shell finite elements. Comput Struct 2004;82(11–12):945–62.
[22] Lee YG, Yoon KH, Lee PS. Improving the MITC3 shell finite element by using the Hellinger–Reissner principle. Comput Struct 2012;110–111:93–106.
[23] Jeon HM, Lee PS, Bathe KJ. The MITC3 shell finite element enriched by interpolation covers. Comput Struct 2014;134:128–42.
[24] Lee Y, Lee PS, Bathe KJ. The MITC3+ shell finite element and its performance. Comput Struct 2014;138:12–23.